Nanostructuring few-layer graphene films with swift heavy ions for electronic application: tuning of electronic and transport properties

Nebogatikova, N. A.; Antonova, I. V.; Erohin, S. V.; Kvashnin, D. G.; Olejniczak, A.; Volodin, V. A.; Skuratov, A. V.; Krasheninnikov, A. V.; Sorokin, P. B.; Chernozatonskii, L. A.;

Originally published:

July 2018

Nanoscale 10(2018), 14499-14509

DOI: https://doi.org/10.1039/c8nr03062f

Nanoscale

Accepted Manuscript

This article can be cited before page numbers have been issued, to do this please use: N. A. Nebogatikova, I. V. Antonova, S. V. Erohin, D. G. Kvashnin, A. Olejniczak, V. A. Volodin, V. Skuratov, A. V. Krasheninnikov, P. B. Sorokin and L. A. Chernozatonskii, *Nanoscale*, 2018, DOI: 10.1039/C8NR03062F.

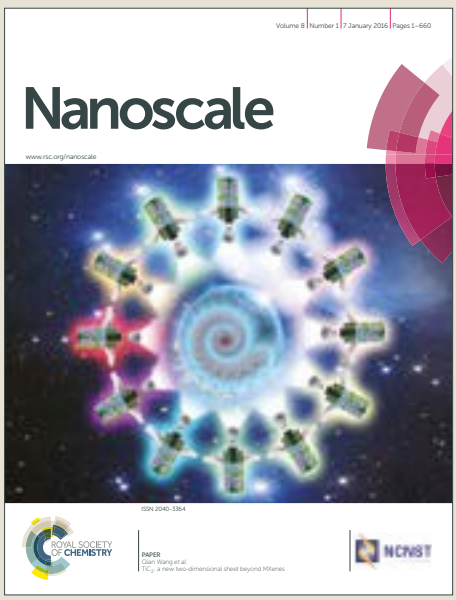

This is an Accepted Manuscript, which has been through the Royal Society of Chemistry peer review process and has been accepted for publication.

Accepted Manuscripts are published online shortly after acceptance, before technical editing, formatting and proof reading. Using this free service, authors can make their results available to the community, in citable form, before we publish the edited article. We will replace this Accepted Manuscript with the edited and formatted Advance Article as soon as it is available.

You can find more information about Accepted Manuscripts in the author guidelines.

Please note that technical editing may introduce minor changes to the text and/or graphics, which may alter content. The journal's standard Terms & Conditions and the ethical guidelines, outlined in our author and reviewer resource centre, still apply. In no event shall the Royal Society of Chemistry be held responsible for any errors or omissions in this Accepted Manuscript or any consequences arising from the use of any information it contains.

ROYAL SOCIETY OF CHEMISTRY

rsc.li/nanoscale

View Article Online
DOI: 10.1039/C8NR03062F

Nanoscale

ARTICLE

Nanostructuring few-layer graphene films by swift heavy ions for electronic application: tuning of electronic and transport properties

Received 00th January 20xx,
Accepted 00th January 20xx

DOI: 10.1039/x0xx00000x

www.rsc.org/

N.A. Nebogatikova,*[a] I.V. Antonova,*[a,b,c] S.V. Erohin,[d,e] D.G. Kvashnin,[d,f] A. Olejniczak,[g,h] V.A. Volodin,[a,b] A.V. Skuratov,[g,k,l] A.V. Krasheninnikov, [i,j,b] P.B. Sorokin,*[d,e,f] L.A. Chernozatonskii[f]

The morphology and electronic properties of single and few-layer graphene films nanostructured by the impacts of heavy high-energy ions have been studied. It is found that ion irradiation leads to the formation of nano-sized pores, or antidots, with sizes ranging from 20 to 60 nm, in the upper one or two layers. The sizes of the pores proved to be roughly independent of the energy of the ions, whereas the areal density of the pores increased with ion dose. With increasing ion energy (>70 MeV), a profound reduction in the concentration of structural defects (by a factor of 2 – 5), relatively high mobility values of charge carriers (700 – 1200 $cm^2/V{\cdot}s$) and a transport band gap of about 50 meV were observed in the nanostructured films. The experimental data were rationalized through atomistic simulations of ion impacts onto few-layer graphene structures with thickness matching the experimental samples. We showed that even a single Xe atom with energy in the experimental range produces considerable amount of damage in graphene lattice, whereas high dose ion irradiation allows to propose a high probability of consecutive impacts of several ions into area already amorphized by previous ions, which increase average radius of the pore to match the experimental results. We also found that the formation of "welded" sheets due to interlayer covalent bonds at the edges and, hence, defect-free antidot arrays is likely at high ion energies (above 70 MeV).

Introduction

High energy ions (>1 MeV/nucleon) can be used for local structural modifications of materials. [1–4] Depending on ion energy and material properties, the modifications can occur at the surface of the irradiated samples and in their bulk. Many materials can be subjected to such modifications in a constructive way, including metals, dielectrics, semiconductors, polymers, and ceramics. For example, irradiation of polymer films and their subsequent etching can be used for the preparation of porous track membranes with pore sizes ranging from nanometers to several micrometers, which are widely employed for solution filtration. [1–3,5] Formation of pores in a membrane material after etching becomes possible due to a substantial modification of the material atomic structure that occurs in cylindrical regions along the ion trajectories, the so-called "tracks". [4,6]

During the impacts of high-energy ions, considerable amount of energy is released in track regions over short times. The slowing down of an energetic ion moving in a solid target can be separated into two channels with different mechanisms, which can be referred to as electronic and nuclear stopping. They usually can be described by electronic (S_e) and nuclear (S_n) stopping power, respectively. The nuclear stopping originates from collisions between the ion and nuclei of the target atoms partially screened by the core electrons. The energy loss is determined by screened Coulomb interactions and momentum transfer. A common feature is that the nuclear stopping is dominant only for ions of relatively low energy (E_{kin}<100 keV/nucleon). The electronic stopping is governed by inelastic collisions between the ion and the electrons in the target and dominates at higher ion energies. Due to the different mechanisms of conversion of electronic excitations into heat, the electronic structure of the target strongly affects the outcome of the ion impact. In metals, the electronic excitations are delocalized due to the presence of

[a] Rzhanov Institute of Semiconductor Physics, Novosibirsk 630090, Russian Federation
[b] Novosibirsk State University, Novosibirsk 630090, Russian Federation
[c] Novosibirsk State Technical University, Novosibirsk 630073, Russian Federation
[d] National University of Science and Technology "MISIS", Leninsky prospect 4, Moscow 119049, Russian Federation
[e] Technological Institute for Superhard and Novel Carbon Materials, Troitsk, Moscow, 108840, Russian Federation
[f] Emanuel Institute of Biochemical Physics RAS, 4 Kosigin st., Moscow 119339, Russian Federation
[g] Center of Applied Physics, Flerov Laboratory of Nuclear Reactions, Joint Institute for Nuclear Research, Dubna 141980, Russian Federation
[h] Faculty of Chemistry, Nicolaus Copernicus University, Gagarin st. 7, 87-100 Torun´, Poland
[i] Helmholtz-Zentrum Dresden-Rossendorf, Institute of Ion Beam Physics and Materials Research, 01328, Dresden, Germany
[j] Department of Applied Physics, Aalto University, P.O. Box 1100, 00076, Helsinki, Finland
[k] National Research Nuclear University MEPhI, Moscow, Russian Federation
[l] Dubna State University, Dubna, Russian Federation
E-mail: nadonebo@gmail.com, antonova@isp.nsc.ru, pbsorokin@misis.ru

View Article Online
DOI: 10.1039/C8NR03062F

conduction electrons. In insulators, excitations may result in a strong heating of the lattice, and once deposited energy exceeds the threshold value which depends on the material, in the formation of defects inside the cylindrical track regions. For swift heavy ions, structural modifications due to electronic stopping are normally most pronounced in the vicinity of the surface, whereas defects due to nuclear stopping mostly appear at the ends of ion trajectories or ranges, which are typically several micrometers. Due to extreme conditions during conversion of electronic excitations into heat, processes that normally proceed at high pressures and elevated temperatures may occur. For instance, two such examples for graphite are the transition of carbon atoms from sp^2 to sp^3 hybridized state and the local formation of nanodiamonds in a graphite matrix. [7–9]

The study of the surfaces of irradiated materials shows that, generally, the surface roughness increases, and various topographic features such as craters or hillocks form on the surface. [10] The formation processes of large structural surface defects are rather complex; however, a sharp threshold dependence on ion energy and, in some cases, phase transitions (melting, etc.) that occur at the surface of materials under irradiation are typical for those processes. [10] During the irradiation of graphite samples with ions whose energy varies from 100 MeV to 1.5 GeV, hillocks were formed on the surface of the samples. The height of the hillocks varied from 0.3 to 0.9 nm, and their mean diameter from 2 to 3.5 nm. Interestingly and importantly, the characteristic sizes of surface defects proved to be nearly independent of the type of the ions and S_e values. [11] Moreover, Liu et al. [11] have shown that threshold value of S_e for damage creation in graphite surface is 7.2 keV/nm, in agreement with theoretical predictions. [12] At lower values of S_e (and a smaller heat release in the target material) no significant structural changes were detected. For the range of ionization losses from 9 to 18 keV/nm, the number of nano-hillocks formed as a function of S_e exhibited a dependence with saturation, i.e., the probability of hillock formation at the HOPG surface reached 1 only for S_e values higher than 18 keV/nm. Based on these observations, the authors predicted that swift heavy ion irradiation of graphite does not result in formation of "classical" tracks, but rather leads to discontinuous randomly distributed amorphous regions.

Apart from microscopy, Raman scattering has emerged as rather powerful and informative tool for studying the structural transformations [7,13,14] that occur in irradiated graphite and graphene films. In the Raman spectrum of irradiated graphite and graphene samples an emergence of D peak (~1360 cm^{-1}) and D' peak (~1624 cm^{-1}) can be detected. [13–15] Both D and D' are second-order defect-induced bands that require symmetry violation (presence of defects) for their activation. The difference is that D-band results from an inter-valley process (the phonon of A_1' symmetry) whereas D'-band originates from intra-valley scattering (E_{2g} symmetry). In a typical experiment, the D'-band detection requires a higher concentration of defects due to small D'-peak intensity. A theoretical explanation why the D'-band intensity is typically weaker than that of the D-band was provided by analyzing the angular dependence of the scattering vectors. Several studies also showed that D to D'-band intensity ratio ($I_D/I_{D'}$) depends on the nature of defects, for example, $I_D/I_{D'} \sim 3$ for sp^3-type defects, ≈7 for vacancies, and ~3.5 for boundaries. [16,17] According to Raman spectroscopy data [13] the ion dose at which the presence of defects can be detected was much lower for graphene than for graphite ($<1\times10^{11}$ vs. 2.5×10^{12} ion/cm^2 for graphene and graphite, respectively). Besides, the different ratios between the intensities of D- and D'-peaks suggest that different structural defects form in graphite and single layer graphene under identical irradiation conditions.

The evolution of the electrical properties of single-layer graphene and few-layer graphene films irradiated with high-energy ions still remains a poorly studied matter. While the literature on the response to irradiation of graphene is vast, the data on the resistance growth, on the change of conductivity type, and on the profound reduction of charge-carrier mobility in graphene samples irradiated with low-energy ions (30-keV Ga+ ions and 5-MeV H+ ions) were only reported. [14,18] On irradiation of graphene films with protons to a dose of 2×10^{15} proton/cm^2, formations of structural defects with dangling bonds in the films were reported. [18] On interaction with atmosphere, the dangling bonds can absorb molecules of various gases and water. Ko et al. [18] expressed an opinion that, due to the Coulomb interaction, the absorbed molecules can act as scattering centers for charge carriers, pointing out that one of possible applications of graphene can be gas and humidity sensors.

In the present study, we irradiated graphene and few-layer graphene films with high-energy heavy ions and observed the formation of nanosized pores (antidots) in the upper layers of the films (1 or 2 monolayers). We observed that increasing ion energy gives rise to a profound reduction in the number of structural defects. The ion-nanostructured graphene layers were found to exhibit a strong dependence of charge-carrier mobility upon ion energy. A possibility of a band gap opening in such structures due to the introduction of antidot arrays with reconstructed (defect-free) "welded" edges was demonstrated, and a theoretical model for this process was proposed.

Methods

Experiment

Single and few-layer graphene films up to 3 nm thick were prepared by electrostatic exfoliation of graphite on 300-nm SiO_2/Si substrates. [19–22] Practically, all samples contained parts with a thickness of 1-2 monolayers, but the main part of the samples were 2-3 nm thick. About 40 samples in total were studied. For changing the morphology of the samples, the irradiation of samples with Xe ions was used. To avoid complete heating of the irradiated targets, the ion flux density was maintained in the range from 2×10^8 to 5.7×10^8 $cm^{-2}\cdot s^{-1}$. The irradiations were carried out at room temperature in

View Article Online
DOI: 10.1039/C8NR03062F

vacuum, at a pressure of $6.3 \cdot 10^{-6}$ Torr. The ion energy was varied in the range from 26 to 167 MeV, and the irradiation dose in the range from 5×10^{9} to 5×10^{12} ion/cm^2. The irradiations were performed on the ion beam line for applied research at the IC-100 cyclotron of FLNR JINR, Dubna.

For examining the properties of the pristine (non-irradiated) and irradiated films, the following experimental techniques were used: optical microscopy, atomic force microscopy (AFM), scanning electron microscopy (SEM), Raman light scattering, along with the electronic transport measurements. Micro-Raman spectroscopy measurements were carried out under ambient conditions at room temperature using the 514.5-nm (2.41-eV) excitation line of an argon ion laser. The laser power shone onto the sample was restricted to 2–3 mW to avoid laser-induced heating. The Raman spectra were recorded in back-scattering geometry. For this purpose, a triple T64000 Horiba Jobin Yvon spectrometer equipped with a micro-Raman setup was used. The spectra were registered in Z(XY)Z polarization geometry: the polarizations of incident and scattered light were perpendicular to each other. A Solver PRO NT-MDT scanning microscope was employed for taking AFM images from the surface of examined films and substrates and for evaluating the sample thicknesses. The measurements were carried out in contact and semi-contact modes. The rounding radius of the used probe never exceeded 10 nm; normally, it was equal to ~2-3 nm. Apart from the study of the surface relief, measurements in lateral-force (friction-force) mode were carried out for visualization of regions differing in their chemical compositions. The current-voltage characteristics were measured with a Keithley picoamperemeter (model 6485) on film samples provided with two contacts prepared from silver alloy. The silver alloy was applied onto the film surface and, then, the sample was annealed at a temperature of 125^{o}C for 20 min to remove the polymer component from the alloy. SEM images were obtained using a JEOL JSM-7800F scanning electron microscope in which the energy of primary electrons was equal to 2 keV.

Q-DLTS measurements were performed using an ASEC-03 DLTS spectrometer for the analysis of carrier emission times as functions of temperature. We varied the time window τ_m while keeping the temperature unchanged. Then, we had $\tau_m = (t_2 - t_1)/\ln(t_2/t_1)$, where t_1 and t_2 are the times at which the Q-DLTS signal (due to the relaxation of the dielectric-trapped charge $\Delta Q = Q(t_2) - Q(t_1)$) was measured after the end of the filling pulse. The examined temperatures ranged from 80 to 350 K.

Atomistic Simulations

The interpretation of the experimental results through atomistic simulations requires proper treating of dynamic energy exchange between electronic and ionic subsystems in the irradiated system. To achieve this, we used a two-temperature molecular dynamics model in which atomic subsystem is described by classical molecular dynamics simulations, whereas electronic subsystem is characterized by local electronic temperature and treated as a continuum on a regular grid. The model accounts for energy transfer between these subsystems. For the calculations we used the LAMMPS code. [23]

Heat transfer between the electronic and atomic subsystems is carried out via an inhomogeneous Langevin thermostat. Energy transport within the electronic subsystem is described according to the heat diffusion equation with added source terms for heat transfer between the subsystems:

$$C_e \frac{\partial T_e}{\partial t} = \nabla (k_e \nabla T_e) - g_p (T_e - T_i) \quad (1)$$

where C_e is the electronic specific heat, k_e is the electronic thermal conductivity, g_p is the coupling constant for the electron-ion interaction. Second term in the right side of the equation represents energy exchange with the atomic system energy due to the temperature difference between the atomic (T_i) and electronic (T_e) subsystems.

The electronic specific heat was obtained from Ref. 24 and expressed in polynomial form:

$$C_e = C_0 + \sum_{n=0}^{4} (10^{-3} T_e)^n a_n \exp(-A T_e^2), \quad (2)$$

The important parameter in the model is electronic thermal conductivity of graphene, which cannot be obtained directly from the experimental data [25] because the measured values are not relevant for energy dissipation during swift heavy ion impacts. In the model k_e is proportional to the electronic specific heat C_e and thermal diffusivity D_e. Using the experimental value of thermal diffusivity leads to the high melting threshold of graphene and thus the destruction of graphene is not observed. Such behavior was mentioned before in work [26] where thermal diffusivity two orders of magnitude smaller than the experimental value [27] was used. We also adopted this approach. Therefore, electronic thermal conductivity in the presented model varies with respect to temperature from 0.003 W K^{-1}m^{-1} to ~35 W·K^{-1}m^{-1}.

The parameter g_p can be expressed as $g_p = m/\tau_p$, where τ_p is the timescale for energy loss due to electron–ion interactions and m is carbon atom mass. For graphene, the characteristic relaxation time due to the interaction with optical phonons is τ_p ~150 fs, [28] and therefore g_p was set to 80 g·mol^{-1}ps^{-1}.

The main mechanism of energy transfer from high-energy ions to the material being irradiated are the ionization losses. Electronic sopping power was calculated using the TRIM package with the setup matching the experiment. We estimated the ionization losses S_e for graphene from 6 to 17 keV/nm for ion energy in the range from 26 to 167 MeV.

The energy input from an ion irradiation was simulated by setting the initial electron temperature profile in the form of Gaussian distribution in graphene. The simulations comprised two steps. First step was a short two-temperature simulation (~1 ps), during which most of the energy from the electronic subsystem was transferred into the ionic system, because in the case of high-energy heavy ions, the ion passage through the few-layered graphene sample occurs on a sub-fs time scale. Since the phonon relaxation time in graphene is larger than a ps, [29] it is clear that there is not sufficient time to form an equilibrium phonon system before most of the energy has already dissipated away. Therefore, a second step is long

View Article Online
DOI: 10.1039/C8NR03062F

geometry relaxation during which the structural changes in the graphene were observed.

The system used in the simulations consisted of a 60×60 nm^2 four layered graphene sheet of ~800000 atoms with periodic boundary conditions.

Results

The electrostatically exfoliated single-layer and few-layer graphene films were investigated by various methods prior to and after the ion bombardment (Fig. 1). An AFM image of the surface of a few-layer graphene film prior to its irradiation is shown in Fig. 1 (a). In the surface profile of the non-irradiated film, mono-atomic steps are clearly seen (see Fig. 1 (d)). Figs. 1 (b) and (c) show the AFM and SEM scans taken from the surface of few-layer graphene films irradiated respectively with 26- and 167-MeV ions. For both samples, the irradiation dose was 3×10^{11} ion/cm^2. Figs. 1 (e) and (f) show the AFM profiles for Fig. 1 (b). The characteristic size of the pores in Figs. 1 (c), (e), and (f) amounts to ~20-60 nm. From the AFM profiles, it is evident that the characteristic depth of the nanopores for 3 nm thick few-layer graphene films (~10 graphene monolayers) is approximately 0.3-0.7 nm. The latter result means that, during the irradiation of the samples with 26-MeV ions, the pore formation process proceeded in one or two upper monolayers (since the inter-layer separation in few-layer graphene is equal to ~0.35 nm). It should be noted that for films irradiated with 26-MeV ions the pores with a depth of one monolayer are predominated. In the case of irradiation with 167-MeV ions, the pores with a depth of two monolayers are more often observed in the few-layer graphene. The dark spots seen in SEM images are likely associated with the formation of defects (or amorphization) at the surface or in pores because without defects pores with 1-2 monolayers depth should not lead to so strong contrast. The characteristic density of holes on the film surface proved to be ~ 10^{10}-10^{11} cm^{-2}. The total number of pores was proportional to ion dose; yet, it was one order of magnitude smaller than the dose and independent of ion energy. It was found that all pores in all irradiated films were roughly identical in size. A more accurate pore size distribution and the distance between pores as a function of ion energy are shown in Fig. S1 in Supplementary information. The samples can be divided into two groups with similar parameters inside the group: the first group includes samples irradiated with ions having energies of 26 and 46 MeV (pore size ~ 15-20 nm) and the second one, the samples irradiated with ions with energies of 77 and 167 MeV (pore size ~ 24-28 nm). If we compare the pore distance between groups, this parameter for the second group is slightly higher (23-26 nm for $E \geq 77$ MeV). In the case of AFM measurements (Fig. S2 in Supplementary information), pore sizes are slightly higher than those extracted from SEM data. The difference between the sizes of pores in the samples irradiated with 26 MeV and 167 MeV ions is more pronounced (~ 30 and ~60 nm). Determination of the pore spacing distribution in the case of AFM was hampered by large noises on the surface relief.

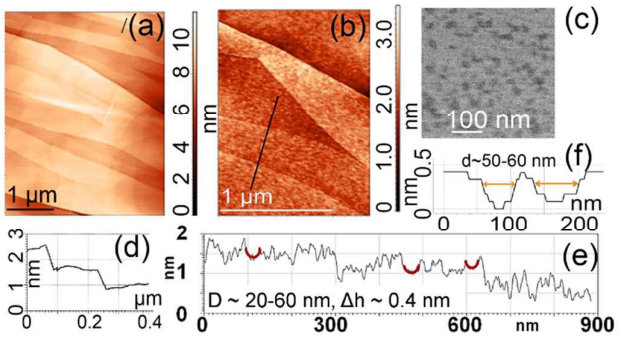

Fig. 1. (a) and (b) AFM images of the surface of pristine and irradiated few-layer graphene film. For irradiation, Xe ions with energy E = 26 MeV were used, and the irradiation dose was 3×10^{11} ion/cm^2. (c) SEM image of a few-layer graphene film irradiated with Xe ions with energy E = 167 MeV; the irradiation dose was 3×10^{11} ion/cm^2. (d) and (e) surface relief profiles of the irradiated and non-irradiated films shown in Figs. (a) and (b); the profiles were taken along the black lines shown in Figs (a) and (b). (f) a fragment of the surface relief profile of an irradiated film with two nanopores. Sample thicknesses vary from a monolayer to 2 -3 nm.

Additional information on the structural changes in the irradiated films was gained using the Raman scattering method. The measurements were performed at an excitation wavelength of 514.5 nm. The Raman spectra of irradiated few-layer graphene films versus ion dose at fixed ion energy are shown in Figs. 2 (a) and (b). In the spectra, the following peaks were observed: the D peak (1360 cm^{-1}), the G peak (1580 cm^{-1}), the D' peak (1625 cm^{-1}), and the 2D peak (2725 cm^{-1}). The G and 2D peaks are normally observed in the Raman spectra of graphene and graphite. However, the relative intensity of the peaks usually exhibits a strong dependence on the number of layers in the films under study. Normally, the D and D' peaks are not observed in the Raman spectra of pristine single and few-layer graphene since, for these materials, in the ideal graphene lattice the selection rules turn out to be violated. Yet, the D and D' peaks may emerge on the introduction of various defects in the film structure. The emergence of a D' Raman peak at ~1620 cm^{-1} may point to the formation of locally compressed regions in the films under study. [30]

With increasing the irradiation dose, the spectral position of D and G peaks displayed a slight blue shift. This observation likely indicates some increase in the rigidity of C-C bonds or emergence of mechanical stresses in the crystal lattice of the irradiated films. Indeed, it was predicted that in the vicinity of defects C-C bonds can increase its rigidity. [31] For instance, strained regions can appear in the vicinity of the formed holes. The blue shift of the G-band for HOPG (from 1580 to 1600 cm^{-1}) occurs for graphite/graphene for low doses, at first stage at the amorphization (for the applied irradiation doses our films are at the first stage). [32] Its origin is not well understood; it might be an "inherent" property of graphite and graphene.

View Article Online
DOI: 10.1039/C8NR03062F

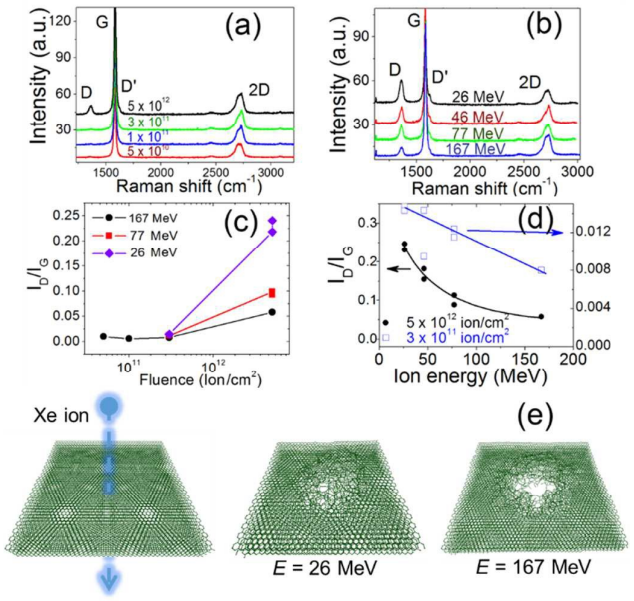

Fig. 2. Raman spectra of ion-irradiated single and few-layer graphene films (a) versus irradiation dose (5×10^{10}-5×10^{12} ion/cm^2) at a fixed ion energy of 167 MeV and (b) versus ion energy in the range of from 26 to 167 MeV at a fixed ion dose of 3×10^{11} ion/cm^2. The thickness of all samples equals to 2-3 nm. (c) The ratio between the intensities of D and G peaks in the Raman spectra of ion-irradiated few-layer graphene films versus ion dose for different ion energies. (d) The ratio between the intensities of D and G peaks in the Raman spectra of ion-irradiated few-layer graphene film versus ion energy for the irradiation doses of 3×10^{11} and 5×10^{12} ion/cm^2. (e) A model of the formation of holes in 4-layered graphene films under the impacts of high-energy ions. Depending on irradiation energy, the formed pores possess various morphologies.

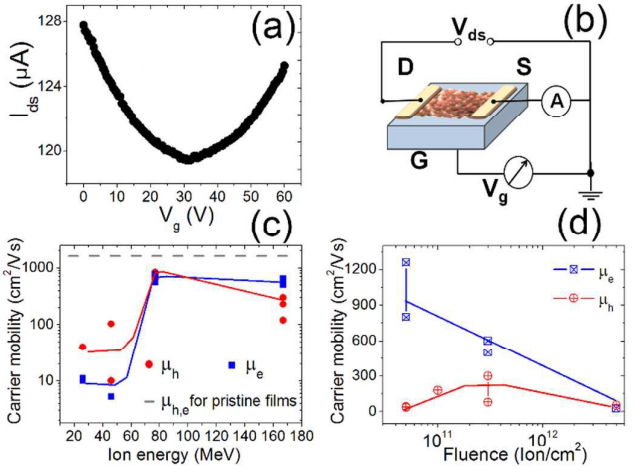

Fig. 3. (a) Dependence of the current I_{DS} on the gate voltage V_g at U_{DS} = 0.2 V for few-layer graphene film irradiated with 77-MeV ions to a dose of 3×10^{11} ion/cm^2. The mobility (720-830 cm^2/V·s) of charge carriers was calculated from measured transient current-voltage characteristics of the films in transistor configuration (see Fig. 3 (b); here, the silicon substrate was used as the gate). The mobility of charge carriers in irradiated few-layer graphene films with a thickness of 2-3 nm versus (c) the ion energy at an irradiation dose of 3×10^{11} ion/cm^2 and (d) the ion dose at ion energy 167 MeV.

With increasing irradiation dose, the defect-induced D Raman peak was found to become more intense. Figs. 2 (c) and (d) show the ratio between the intensities of D and G peaks, I_D/I_G, versus ion dose and ion energy, respectively. Very likely, the increase in the intensity of the D peak with increasing irradiation dose is related to the formation of a larger number of defects in the films. The formation of pores in the films leads to the appearance of edge atoms with dangling bonds in the film structure. The observed dependence of the I_D/I_G ratio on ion energy at a fixed irradiation dose (see Fig. 2 (d)) suggests that a greater amount of defects forms in the structure of graphene films irradiated with lower-energy ions in comparison with high-energy ions. Our atomistic calculations show that depending on ion energy, the pores formed in graphene films differ in the structure (Fig. 2 (e)). Whereas Xe ions with energy E = 26 MeV induces the amorphization of the structure with a large number of defects, high-energy ions (E = 167 MeV) create pronounced pores with the closed structure of the edges, as detailed later in the Discussion section.

Most of the papers consider changes in the position of 2D-band since it is more sensitive to strain. Nevertheless, Raman measurements were made for a set of the irradiated films with different thickness. Therefore, we do not analyze 2D-band shape dependence on the irradiation conditions.

For examining the effects of ion irradiation on the electrical properties of few-layer graphene films, we studied the value of charge-carrier mobility, the temperature dependence of electric current, and the characteristic relaxation time of non-equilibrium charges in irradiated and non-irradiated films. It was found that, as a result of the irradiation of the films with ions under different conditions, nanostructures with fundamentally different electrical properties were formed.

For determining the charge-carrier mobility in the films, measurements of film conductivity in transistor configuration were performed (Fig. 3 and Fig. S3 in Supplementary information). In these measurements, the silicon substrate was used as the gate. The drift field V_{DS} between the source contact and the drain contact was 0.2 V. Depending on sample sizes, the characteristic resistance values in the pristine and irradiated films were ~1.5–5 kOhm (this value somewhat increased in the irradiated material). A typical dependence of the current I_{DS} flowing between the source and the drain on the gate voltage V_G is shown in Fig. 3 (a). Here, the charge-carrier mobility μ was calculated by the following formula: [33,34]

$$\mu = \frac{\Delta I_{DS}}{\Delta V_G} \frac{1}{C_{SiO_2} V_{DS} \frac{W}{L}} \quad (3)$$

In formula (3), C_{SiO_2} is the specific capacitance of the oxide layer on the surface of the silicon substrate (oxide thickness 300 nm, ε ~ 3.9), W and L are the width and length of the few-layer graphene film. In the non-irradiated films, the mobility of charge carriers was equal to 1300-1500 cm^2/V·s. The dependences of charge-carrier mobility on the ion energy and ion dose are shown in Figs. 3 (c) and (d) respectively. In few-layer graphene films irradiated with low-energy ions, the mobility of charge carriers decreased by one or two orders of magnitude, down to 4–100 cm^2/V·s. In the films irradiated with high-energy ions (with energy greater than 70 MeV), the

View Article Online
DOI: 10.1039/C8NR03062F

charge-carrier mobility remained rather high, 600 - 900 $cm^2/V{\cdot}s$, see Fig. 3 (c). As follows from Fig. 3 (d), the holes and electrons exhibit different sensitivities of their mobility to the irradiation dose. The electron mobility decreases in value with increasing the irradiation dose and with the increase in the number of structural defects in the films, see Fig. 3 (d). For pores, a more complex dependence is observed. Such effect can be explained by the different atomic structure of the formed pores. The pores formed by low-energy ions display highly distorted structure with a huge number of scattering centers whereas high-energy ions create pores with pronounced edges, therefore, resulted structure can be represented as a graphene nanomesh into which a high-density array of nanoscale pores are punched. Neighbored pores induce quantum confinement effect in graphene and open small band gap (see discussion below). It is important to mention that electrical properties and, first of all, the carrier mobility of samples irradiated with 167 MeV ions are not degraded with a time as it usually observed for graphene with non-reconstructed pores. For instant, for 167 MeV ion dose of $1{\times}10^{11}$ ion/cm^2 electron mobility measured in a year after irradiation was equal to 1000-1300 $cm^2/V{\cdot}s$.

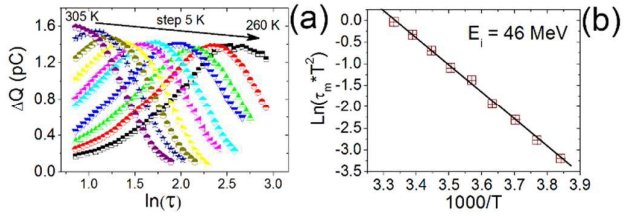

Fig. 4. (a) Q-DLTS spectra and (b) the temperature dependences of the relaxation time of non-equilibrium charges in graphene films irradiated with 46-MeV ions to a dose of $5{\times}10^{12}$ ion/cm^2.

The charge-carrier trapping and emission processes in the irradiated films were studied by means of charge deep-level transient spectroscopy. The properties of the nanostructured films were found to exhibit a strong dependence on the irradiation conditions. In the films irradiated with 46-MeV ions, the processes of charge-carrier capture at electrically active centers were identified (Fig. 4 (a)); those processes manifested themselves in the emergence of peaks observed in the Q-DLTS spectra in the temperature interval from 260 to 305 K. An analysis of the temperature dependence of the characteristic relaxation time of non-equilibrium charges in Arrhenius coordinates (Fig. 4 (b)) has allowed us to determine the activation energy of the traps, which turned out to fall in the interval from 0.51 to 0.54 eV.

In the films irradiated with high-energy ions (167 MeV), no charge-carrier capture processes were detected. The formation of deep-level traps in few-layer graphene films appears to correlate with the observation of defects in the Raman spectra and with the formation processes of dangling bonds in the films.

A different picture was observed while analyzing the temperature dependence of electric current in the irradiated films (see Fig. 5). In the films irradiated with 26- and 46-MeV ions, no variation of electric current with temperature in the temperature range from 80 to 300 K was observed (see Figs. 5 (b) and (c)). In the films irradiated with higher-energy ions, a profound variation of the current in the temperature range from 90 to 300 K was detected (Fig. 5 (a)).

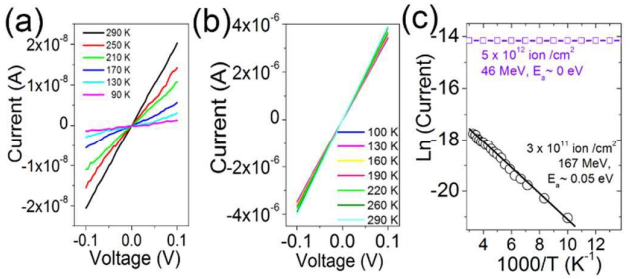

Fig. 5. (a) and (b) Temperature dependence of electric current in graphene films irradiated with 167-MeV ions to a dose of $3{\times}10^{11}$ ion/cm^2 and with 46-MeV ions to a dose of $5{\times}10^{12}$ ion/cm^2. (c) Temperature dependence of electric current in irradiated films shown in an Arrhenius plot. Currents are given without correction on size and thickness parameters of the film. The thickness and width/length relation for 167-MeV irradiated samples are 1.2 nm and 12.5 and for 46-MeV MeV irradiated samples are 3 nm and 2.1.

Discussion

The observed changes in the properties of irradiated films can be attributed to the dependence of the amount of energy lost by the ions during their interaction with the target films on ion energy. The ionization losses prevail over atomic losses in the ion projection range region. We estimated energy losses of both types using TRIM program (Fig. 6). In the present study, the projected ions ranges were in the interval from ~5 to 19.4 μm and, hence, all the ions penetrated deep into the substrate, and it is in the substrate where the main portion of ion-produced defects formed. In should be noted here that, in the examined films, the processes of atom knocks-out from the film occurred when the losses for atomic displacements reached values greater than 5-7 keV/nm. [12] The calculations of the ionization and atomic losses for Xe ions show that the main energy-transfer channel for the nanometer-thick films was the ionization losses, with no direct knocking of carbon atoms out of the films being occurred. In the case of monolayer films and 167-MeV ions, it can be expected that the energy released in graphene will amount to ~ 6 keV, and in the case of 3-nm thick films, to ~ 51 keV. Vázquez et al. [24] examined swift heavy ion-induced defect production in suspended single layer graphene using Raman spectroscopy and a two-temperature molecular dynamics model. The authors showed that an increase in the electronic stopping power of the ion results in an increase in the size of the pore-type defects, with a defect formation threshold at 1.22–1.48 keV/layer or 3.5-4.2 keV/nm. These results allow Vázquez et al. [24] to predict that swift heavy ions can create nanopores in graphene, and that their size can be tuned between 1 and 4 nm diameter by choosing a suitable stopping power.

View Article Online
DOI: 10.1039/C8NR03062F

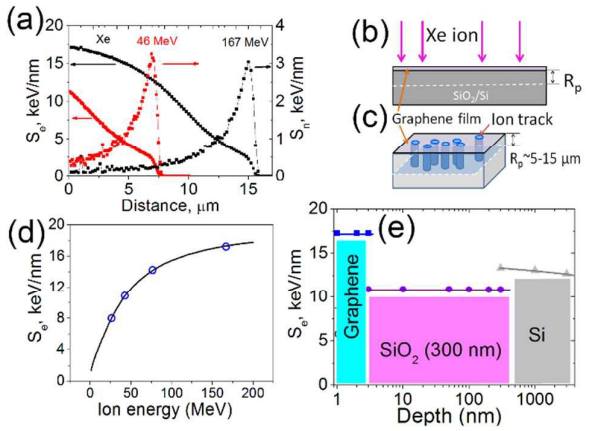

Fig. 6. (a) The calculated energy losses of ions for ionization and atomic displacements in a graphite target under its bombardment with 46- and 167-MeV Xe ions. (b) Schematic representation of the irradiation process of film and substrate. (c) Schematic representation of ion tracks formed in the silicon substrate due to the produced atomic displacements. (d) The ionization losses of high-energy Xe ions on the surface of graphite versus the ion energy as calculated by SRIM. (e) The ionization losses S_e of high-energy Xe ions with initial energy 167 MeV during the penetration of the ions through graphene and few-layer graphene films on oxidized silicon substrates covered with 300-nm thick oxide layer. The ionization losses vary with depth due to the gradual loss of energy by the ions and due to the different values of the losses for different materials.

However in our study the defect formation threshold is overcome for all ions used, and the pore sizes are more than an order of magnitude larger than predicted in Ref. 24. In order to study in detail, the behavior of the lattice under the impacts of ions with such energy and understand the underlying processes we carried out atomistic simulations of irradiation process. We provided direct description of the experimental data by simulation of few-layer graphene of similar thickness (~2 nm, 4 layers) whereas impact of the SiO_2 substrate was modeled by pure repulsive field. We simulated the similar irradiation setup and found that irradiation by only one Xe atom with energy in the experimental range (167 MeV) sufficiently distorts graphene lattice, which leads to formation of a pore with a size of ~5 nm. This result originates from the energy transfer from the electronic to atomic subsystem of graphene with further heating of the lattice and evaporation of carbon atoms.

Despite substantial damage of graphene, the obtained pore is nevertheless smaller than the observed in our experiments. However, the high ion irradiation dose (dose of 5×10^{12} ion/cm^2) allows to propose a high probability of consecutive impacts of several ions into area already amorphized by previous ions. In this case the size of the formed structure linearly increases (Fig. 7 (a)) and after the fifth ion impact the average radius of the pore is getting close to the experimental range.

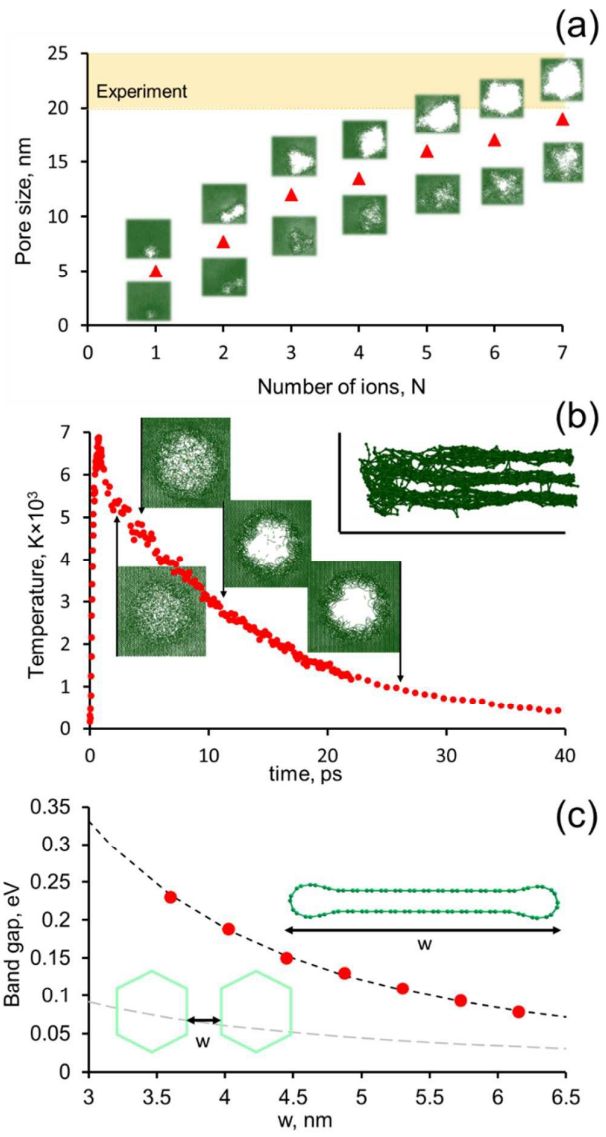

Fig. 7. a) Hole size as a function of the number of Xe ions irradiated considered region. The range of experimental values of the pore size is denoted by orange. Upper and down series of the insets (relatively to the data) represent atomic structures of holes formed by ions with energy 167 and 26 MeV, respectively, b) Temperature and structural changes of three-layered graphene in MD simulations after the irradiation at Xe energy 100 MeV. The evolution of the graphene structure at the chosen steps is shown. In the inset the zoomed side view connected edges is shown. c) Band gap of the infinite ribbon with connected edges as a function of the distance between connected regions (the fitted quantum confinement trend is shown by black dashed curve). The band gap via the region between pores calculated in Ref. 35 is represented by gray dashed curve. The schematic views of corresponding structures are presented in the inset.

The substrate plays an important role in the observed effect. For example, it was demonstrated in Ref. 36 that irradiation of freestanding bilayer graphene leads to plow up of the pore edges, whereas our simulations show that the confinement of the graphene from one side leads to spoiling of the atoms to the one direction with stimulating of connection of neighbored layers. This agrees with the previous observations of the

View Article Online
DOI: 10.1039/C8NR03062F

"geometrical" effects of the substrate on the evolution of displaced atoms during irradiation of supported graphene. [37] Strong local heating of SiO_2 substrate (up to 1500 – 3000°C) that takes place in the picosecond time-scale (10^{-12} – 10^{-11}) [38] can possibly stimulate a pronounced increase in pore size.

The high temperature in the irradiated region leads to the evaporation of carbon with the formation of the pores, see Fig. 7 (b). We can suggest that this effect is mostly pronounced on the surface, where the atoms evaporate, whereas underneath layers can mostly keep the atomic structure and further heal the defects. [39] This can explain the observation of very shallow pores. The free edges of the neighbored graphene layers tend to connect with each other in order to minimize the edge energy. This effect is quite common and was observed in bilayered graphene, [40] graphite filaments, [41] multi-wall carbon nanotubes, [42,43] graphite [44] and nanographite [45] cases. It was shown [35] that at least in the case of bilayer graphene such process in energetically favorable and connection of the edges proceeds without any energy barrier. As a result, the formation of a nanostructured bilayer-graphene film with a number of sp^3-hybridized atoms turns out to be possible.

We studied the electronic properties of the perfect system when graphene layers seamlessly connect with each other. Such nanostructures combine the flat geometry of graphene with the curvature of small diameter nanotubes at the edges and can display semiconductor and metallic properties depending of the atomic geometry. [35,46,47] The main advantageous feature of such structures in comparison with the structures traditionally fabricated by means of nanolithography consists in the possibility of realization of a high mobility of charge carriers due to the absence of charge-carrier scattering at edge atoms. Namely, nanomeshes consisting of graphene with closed edges can display high transport characteristics as suggested by wave-packet dynamical calculations of antidots arrays in bilayered graphene [35] showing a high transmission probability of charge carriers. Therefore, graphene with closed edges can couple together high conducting properties of carbon nanotubes and controllable electronic properties of graphene ribbons which makes possible the fabrication of perfect two-dimensional conductors for future nanoelectronics.

Even though the bilayer graphene with periodically arranged pores with closed edges is a perfect model which cannot directly correspond to the sample obtained in experiment, the opening of band gap due to quantum confining by closed edges probably has the real basis. The theory considered previously only relatively small pores of nanometer sizes. [35,47] They properties can be sufficiently different from the nanostructures studied in this work. We considered here the dependence of band gap of bilayer graphene with closed edges on the width w of the flat graphene between edges. We found that band gap of such structure monotonously decreases as w increases. We fit these band gap values with a function of A/w^{α}, where A = 3.024 eV·nm^2 and α is found to be 2, which exactly corresponds to an effective-mass particle-in-a-box behavior. The obtained trend clearly manifests that even at the experimentally measured distances between neighbored holes of 10 nm the structures display the value of band gap of ~10 meV, which agrees well with the experimental data given below. Also, these estimations are supported by our previous data [35] obtained for the bilayer graphene with periodically arranged hexagonal holes. Band gap of such nanostructures depends on the distance between neighbored holes as $A'/w^{\alpha'}$, where A' = 0.43 eV·nm^2 and α' = 1.41 (shown by gray dashed line in Fig. 7(c). At experimentally measured distances 10 nm such trend also gives ~10 meV.

It is worth noting that the electronic transport properties of graphene films irradiated with ions with different energies (Fig. 3 (c)) change drastically at a critical ion energy of 70 MeV (S_e ~ 14 keV/nm). At higher ion energies (above 70 MeV) and low irradiation doses (lower than 3×10^{11} ion/cm^2), the mobility of charge carriers weakly differs from the charge-carrier mobility in the pristine films. Fig. 6 (a) shows the calculated losses for ionization and for the production of atomic displacements in a graphite target for Xe ions with energies 46 and 167 MeV. The dependence of ionization losses on the ion energy is shown in Fig. 6 (c). The mobility of charge carriers is a parameter exhibiting a very high sensitivity to the structural perfection of the film. A high mobility of charge carriers in the layers irradiated with ions having energy above 70 MeV points to a smaller amount of irradiation induced defects, and this finding fairly well correlates with the Raman data. It appears that a reconstruction of dangling bonds in different graphene sheets occurs in bi-layer graphene films at ion energies exceeding this threshold value (S_e = 14 keV/nm) yielding "welded" nanopore joints. Also to be taken in consideration is the fact that one formed pore corresponds to approximately ten ions that have impinged the film. All in all, an amount of energy roughly equal to 140 keV is locally absorbed in bi-layer graphene to yield one pore with the reconstructed edges. To complete the picture, we have to note here that such structures most likely demonstrate an opening of a 50-meV transport band gap and no occurrence of electrically active defects in the films as revealed by the Q-DLTS data.

During irradiation of the films with lower-energy ions (S_e < 14 keV/nm), according to the Raman data, the formation of pore edges with dangling bonds occurs, followed by subsequent oxidation of film edges. According to the Q-DLTS data, such structures contain electrically active defects with activation energy ~0.52 eV, have a metallic conductivity, and contain no forbidden energy ranges in their band structure.

Simultaneously, a profound reduction of hole mobility in graphene films irradiated with low ion doses was observed (Fig. 3 (d)). The reduction of hole mobility can be related to the formation of highly amorphous regions whereas increasing of ion energy leads to the formation of the pores with pronounced edges (compare atomic structures of pores created by Xe ion with energy 26 MeV and 167 MeV, see Fig. 2 (e). Therefore, the effects of ion irradiation with low and high energies on the atomic structure and therefore electronic properties of the films are substantially different. The pore with dangling bonds can be considered as the only scattering center (the irradiation of low energy ions can be roughly

View Article Online
DOI: 10.1039/C8NR03062F

represented as amorphization of the film), whereas the pore with connected edges (created by high-energy ions) can be referred to as the boundary for the charge carriers. Neighbored pores confine the graphene region, which leads to band gap opening and formation of preferred direction for charge transport with high mobility.

The effect of antidot lattice (30 nm antidots with 30 nm neck width between them) created in graphene by means of the electron beam on carrier transport was analyzed by Mackenzie. [48] The carrier mobility decreased after nanostructuring from 300 to 5÷100 $cm^2/V{\cdot}s$ depending on the number of antidot lines. Such value for carrier mobility is rather small as compared to that in the pristine graphene obtained by micromechanical exfoliation approach and then transferred onto SiO_2 substrate, but it is typical for nanostructured graphene devices. Low carrier mobility for nanostructured graphene is usually caused by the negative influence of the scattering edge atoms and adsorbed functional groups. The dependence of carrier mobility on antidot number in [48] is shown to be the same as that for the hole mobility in our investigation.

A similar effect of mobility decreasing was observed when single-layer graphene samples were nanostructured with the use of block copolymers. [49,50] The decrease in mobility for such nanostructured graphene films was much more pronounced (from 700 to 200 $cm^2/V{\cdot}s$) than for those prepared from bi-layer graphene (from 730 to 530 $cm^2/V{\cdot}s$). Oh et al. [50] did not discuss this difference, but it can be assumed that oxygen plasma treatment and high temperature annealing used in their study led to a partial reconstruction of nanopores in bi-layer graphene.

Electrical and structural properties of the graphene films irradiated with 30-35 keV Ga^+ and C^+ ions in the dose range of 10^{11} to 10^{15} ion/cm^2 were investigated in Refs. 14,32. The transition to a carrier hopping transport was found in both studies [14,32] for high irradiation dose (~10^{13}-10^{14} ion/cm^2). Such a change in the electrical properties is usually caused by an appearance of charge-carrier strong scatters in the graphene structure. In our investigation, we found similar centers for films irradiated by ions with $E < 70$ MeV ions. Usually, it is suggested that the effect is related to dangling bonds and edge atom formation.

Conclusions

The structure and properties of few-layered graphene samples nanostructured by irradiating them with high-energy heavy ions (Xe ions with energies from 26 to 167 MeV, ion doses 3×10^{10} to 3×10^{12} ion/cm^2) were investigated. It was found that ion irradiation leads to the formation of nanopores with sized of from 20 to 60 nm in the upper layers of few-layered graphene samples (1-2 monolayers). The sizes of the pores were roughly independent of the energy and dose of the ions. The number of pores was directly proportional to ion dose with a coefficient of 0.1. It was found that, with increasing ion energy, there occurred a profound reduction in the concentration of structural defects. For instance, according to the Raman data, the ratio between the intensity of the defect-induced D peak and the intensity of the G peak decreased by a factor of 2 – 5 with increasing ion energy from 26 to 167 MeV. By means of charge deep-level transient spectroscopy, it was found that in the structures irradiated with 26-MeV ions electrically active defects with 0.52-eV activation energy were observed, whereas no electrically active defects were detected in the structures irradiated with 167-MeV ions. It was demonstrated that, depending on ion energy, one can obtain nanostructured graphene layers with different charge-carrier mobility values in the layers. For instance, in layers irradiated with less than 70-MeV ions the charge-carrier mobility was found to fall in the range from 1 to 100 $cm^2/V{\cdot}s$, whereas in graphene layers irradiated with higher-energy ions, 77 to 146 MeV, the mobility was in the range of 700 – 1200 $cm^2/V{\cdot}s$ (at ion doses of $(1\text{-}3)\times10^{11}$ ion/cm^2). Before irradiation, the mobility value in those layers was 1000 – 1500 $cm^2/V{\cdot}s$. The possibility of opening a band gap of about 50 meV in the nanostructured samples irradiated with 167-MeV Xe ions due to the introduction of an array of antidots with reconstructed edges has most likely been observed. The experimental findings were rationalized through atomistic simulations. We predicted that even single Xe atom with energy in the experimental range produces considerable amount of damage in graphene lattice whereas the high ion irradiation dose (5×10^{12} ion/cm^2) allows to propose a high probability of consecutive impacts of several ions into area already amorphized by previous ions and increasing of average radius of the pore to the experimental range. Also, it was found that at high energies (above 70 MeV), the formation of "welded" sheets due to interlayer covalent bonds at the edges and, hence, defect-free antidot arrays in few-layer graphene are possible at certain irradiation conditions, possibly with using an overlay system with periodic holes as a mask.

Conflicts of interest

There are no conflicts to declare

Acknowledgments

The authors are thankful to Dr. S.A. Smagulova for the possibility to do Q-DLTS measurements. Simulations of graphene irradiation (S.V.E., D.G.K. and P.B.S.) were supported by the Russian Science Foundation (Project identifier: 17-72-20223). A.V.K. acknowledges the financial supports of the Ministry of Education and Science of the Russian Federation in the framework of Increase Competitiveness Program of NUST "MISiS" (No. K3-2017-021). D.G.K. (electronic structure calculations) acknowledges the grant of the president of Russian Federation for government support of young Ph.D. scientists (MK-3326.2017.2). N.N.A. acknowledges the financial supports of RFBR (No. 18-32-00449) and grant of the president of Russian Federation for government support of young Ph.D. scientists (SP-5416.2018.2). L.A.C. (study of models) acknowledges the financial support of RFBR 17-02-01095. We

View Article Online
DOI: 10.1039/C8NR03062F

also thank CSC-IT Center for Science Ltd., Finland for generous grants of computer time.

Notes and references

1 D. Fink, L. T. Chadderton, K. Hoppe, W. R. Fahrner, A. Chandra and A. Kiv, *Nucl. Instrum. Methods Phys. Res. Sect. B Beam Interact. Mater. At.*, 2007, **261**, 727–730.
2 A. Schulz, G. N. Akapiev, V. V. Shirkova, H. Rösler and S. N. Dmitriev, *Nucl. Instrum. Methods Phys. Res. Sect. B Beam Interact. Mater. At.*, 2005, **236**, 254–258.
3 H. Hanot and E. Ferain, *Nucl. Instrum. Methods Phys. Res. Sect. B Beam Interact. Mater. At.*, 2009, **267**, 1019–1022.
4 G. N. Akapiev, S. N. Dmitriev, B. Erler, V. V. Shirkova, A. Schulz and H. Pietsch, *Nucl. Instrum. Methods Phys. Res. Sect. B Beam Interact. Mater. At.*, 2003, **208**, 133–136.
5 P. Apel, *Nucl. Instrum. Methods Phys. Res. Sect. B Beam Interact. Mater. At.*, 2003, **208**, 11–20.
6 A. V. Mitrofanov, P. Yu. Apel, *Nucl. Instrum. Methods Phys. Res. Sect. B Beam Interact. Mater. At.*, 2006, **245**, 332–336.
7 A. V. Krasheninnikov and K. Nordlund, *J. Appl. Phys.*, 2010, **107**, 071301–071370.
8 T. L. Daulton, M. A. Kirk, R. S. Lewis and L. E. Rehn, *Nucl. Instrum. Methods Phys. Res. Sect. B Beam Interact. Mater. At.*, 2001, **175–177**, 12–20.
9 A. Dunlop, G. Jaskierowicz, P. M. Ossi and S. Della-Negra, *Phys. Rev. B*, 2007, **76**, 155403.
10 F. Aumayr, S. Facsko, A. S. El-Said, C. Trautmann and M. Schleberger, *J. Phys. Condens. Matter*, 2011, **23**, 393001.
11 J. Liu, R. Neumann, C. Trautmann and C. Müller, *Phys. Rev. B*, 2001, **64**, 184115.
12 O. Ochedowski, O. Lehtinen, U. Kaiser, A. Turchanin, B. Ban-d'Etat, H. Lebius, M. Karlušić, M. Jakšić and M. Schleberger, *Nanotechnology*, 2015, **26**, 465302.
13 J. Zeng, H. J. Yao, S. X. Zhang, P. F. Zhai, J. L. Duan, Y. M. Sun, G. P. Li and J. Liu, *Nucl. Instrum. Methods Phys. Res. Sect. B Beam Interact. Mater. At.*, 2014, **330**, 18–23.
14 Y.-B. Zhou, Z.-M. Liao, Y.-F. Wang, G. S. Duesberg, J. Xu, Q. Fu, X.-S. Wu and D.-P. Yu, *J. Chem. Phys.*, 2010, **133**, 234703.
15 A. C. Ferrari and J. Robertson, *Phys. Rev. B*, 2000, **61**, 14095–14107.
16 A. Zandiatashbar, G.-H. Lee, S. J. An, S. Lee, N. Mathew, M. Terrones, T. Hayashi, C. R. Picu, J. Hone and N. Koratkar, *Nat. Commun.*, 2014, **5**, 3186–3194.
17 A. Eckmann, A. Felten, A. Mishchenko, L. Britnell, R. Krupke, K. S. Novoselov and C. Casiraghi, *Nano Lett.*, 2012, **12**, 3925–3930.
18 G. Ko, H.-Y. Kim, F. Ren, S. J. Pearton and J. Kim, *Electrochem. Solid-State Lett.*, 2010, **13**, K32–K34.
19 A. N. Sidorov, M. M. Yazdanpanah, R. Jalilian, P. J. Ouseph, R. W. Cohn and G. U. Sumanasekera, *Nanotechnology*, 2007, **18**, 135301.
20 N. A. Nebogatikova, I. V. Antonova, V. A. Volodin and V. Y. Prinz, *Phys. E Low-Dimens. Syst. Nanostructures*, 2013, **52**, 106–111.
21 N. A. Nebogatikova, I. V. Antonova, V. Y. Prinz, V. B. Timofeev and S. A. Smagulova, *Carbon*, 2014, **77**, 1095–1103.
22 I. V. Antonova, N. A. Nebogatikova and V. Y. Prinz, *Appl. Phys. Lett.*, 2014, **104**, 193108.
23 S. Plimpton, *J. Comput. Phys.*, 1995, **117**, 1–19.
24 H. Vázquez, E. H. Åhlgren, O. Ochedowski, A. A. Leino, R. Mirzayev, R. Kozubek, H. Lebius, M. Karlušic, M. Jakšic, A. V. Krasheninnikov, J. Kotakoski, M. Schleberger, K. Nordlund and F. Djurabekova, *Carbon*, 2017, **114**, 511–518.
25 S. Yiğen, V. Tayari, J. O. Island, J. M. Porter and A. R. Champagne, *Phys. Rev. B*, 2013, **87**, 241411.
26 V. V. Pisarev and S. V. Starikov, *J. Phys. Condens. Matter*, 2014, **26**, 475401.
27 H. Cabrera, D. Mendoza, J. L. Benítez, C. B. Flores, S. Alvarado and E. Marín, *J. Phys. Appl. Phys.*, 2015, **48**, 465501.
28 J. C. Johannsen, S. Ulstrup, F. Cilento, A. Crepaldi, M. Zacchigna, C. Cacho, I. C. E. Turcu, E. Springate, F. Fromm, C. Raidel, T. Seyller, F. Parmigiani, M. Grioni and P. Hofmann, *Phys. Rev. Lett.*, 2013, **111**, 027403.
29 K. Kang, D. Abdula, D. G. Cahill and M. Shim, *Phys. Rev. B*, 2010, **81**, 165405.
30 M. A. Bissett, M. Tsuji and H. Ago, *Phys. Chem. Chem. Phys.*, 2014, **16**, 11124–11138.
31 D. G. Kvashnin and P. B. Sorokin, *J. Phys. Chem. Lett.*, 2015, **6**, 2384–2387.
32 G. Buchowicz, P. R. Stone, J. T. Robinson, C. D. Cress, J. W. Beeman and O. D. Dubon, *Appl. Phys. Lett.*, 2011, **98**, 032102.
33 F. Schwierz, *Nat. Nanotechnol.*, 2010, **5**, 487–496.
34 J.-S. Moon, K. Gaskill and P. Campbell, , DOI:10.5772/16102.
35 D. G. Kvashnin, P. Vancsó, L. Y. Antipina, G. I. Márk, L. P. Biró, P. B. Sorokin and L. A. Chernozatonskii, *Nano Res.*, 2015, **8**, 1250–1258.
36 D.-D. Zhao, *J. Comput. Theor. Nanosci.*, 2017, **14**, 485–489.
37 M. Kalbac, O. Lehtinen, A.V. Krasheninnikov and J.K. Keinonen, *Adv. Mater.*, 2013, **25**, 1004–1009.
38 M. Toulemonde, C. Dufour, A. Meftah and E. Paumier, *Nucl. Instrum. Methods Phys. Res. Sect. B Beam Interact. Mater. At.*, 2000, **166–167**, 903–912.
39 R. Zan, Q. M. Ramasse, U. Bangert and K. S. Novoselov, *Nano Lett.*, 2012, **12**, 3936–3940.
40 Z. Liu, K. Suenaga, P. J. F. Harris and S. Iijima, *Phys. Rev. Lett.*, 2009, **102**, 015501–015504.
41 H. Murayama and T. Maeda, *Nature*, 1990, **345**, 791.
42 Y. Rotkin and Y. Gogotsi, *Mater. Res. Innov.*, 2002, **5**, 191–200.
43 J.A. Rodríguez-Manzo, A.V. Krasheninnikov and F. Banhart, *ChemPhysChem*, 2012, **13**, 2596–2600.
44 K. Moriguchi, S. Munetoh, M. Abe, M. Yonemura, K. Kamei, A. Shintani, Y. Maehara, A. Omaru and M. Nagamine, *J. Appl. Phys.*, 2000, **88**, 6369–6377.
45 P. Tan, S. Dimovski and Y. Gogotsi, *Philos. Trans. R. Soc. Lond. Math. Phys. Eng. Sci.*, 2004, **362**, 2289–2310.
46 L. A. Chernozatonskii, V. A. Demin and A. A. Artyukh, *JETP Lett.*, 2014, **99**, 309–314.
47 L. A. Chernozatonskii, V. A. Demin and P. Lambin, *Phys. Chem. Chem. Phys.*, 2016, **18**, 27432–27441.
48 D. M. A. Mackenzie, A. Cagliani, L. Gammelgaard, B. S. Jessen, D. H. Petersen and P. Bøggild, *Int. J. Nanotechnol.*, 2017, **14**, 226–234.
49 M. Kim, N. S. Safron, E. Han, M. S. Arnold and P. Gopalan, *Nano Lett*, 2010, **10**, 1125–1131.
50 J. Oh, H. Yoo, J. Choi, J. Y. Kim, D. S. Lee, M. J. Kim, J.-C. Lee, W. N. Kim, J. C. Grossman, J. H. Park, S.-S. Lee, H. Kim and J. G. Son, *Nano Energy*, 2017, **35**, 26–35.